JFM RAPIDS
journals.cambridge.org/rapids

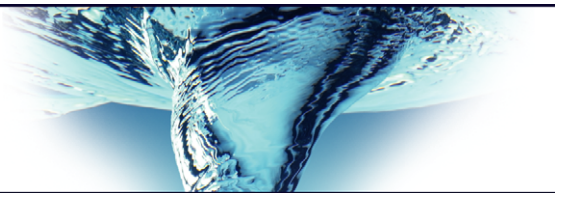

Halting scale and energy equilibration in two-dimensional quasigeostrophic turbulence

R. K. Scott† and D. G. Dritschel

School of Mathematics and Statistics, University of St Andrews, North Haugh, St Andrews KY16 9SS, UK

(Received 23 October 2012; revised 17 January 2013; accepted 23 February 2013)

The halting scale of the inverse energy cascade and the partition between kinetic and potential energy are considered for the case of forced quasigeostrophic turbulence in the regime of intermediate Rossby deformation length, for which the deformation length is comparable to the energy-containing scales of the flow. Phenomenological estimates for the halting scale and equilibrated energy of the forced–dissipative system with a simple representation of large-scale thermal damping are tested against numerical integrations and are found to poorly describe the numerically obtained dependence on damping coefficient; a modified scaling law is proposed that more accurately describes the dependence. The scale-selective nature of the damping leads to a large-scale spectral bottleneck that steepens the energy spectrum, consistent with previous studies of hypodiffusive dissipation. It is found that, across the parameter range considered, the blocking is largely insensitive to the ratio of deformation radius to the energy-containing scales.

Key words: geophysical and geological flows, geostrophic turbulence, quasi-geostrophic flows

1. Introduction

This paper examines the equilibration of energy in the two-dimensional quasigeostrophic equations (e.g. Vallis 2006), arguably the simplest description of the large-scale, low-frequency motion of planetary atmospheres and oceans that allows for free-surface effects and a representation of the gravitational restoring force. The system arises also in the theory of drift-wave turbulence in a magnetically confined plasma (Hasegawa & Mima 1978). Free-surface effects introduce two main complications into the simple two-dimensional barotropic model: an extra length scale, the Rossby deformation length $L_D = \sqrt{gH}/f$, where g is the gravitational acceleration, H is the mean layer depth, and f is the Coriolis parameter, that measures the relative effects of gravitation and rotation; and a partition of the fluid energy into kinetic

† Email address for correspondence: rks@mcs.st-and.ac.uk

doi:10.1017/jfm.2013.120

and potential components. The introduction of the extra length scale fundamentally alters the properties of turbulence in the system, while the partition into kinetic and potential energies renders inadequate the predictions of energy equilibration available from two-dimensional barotropic theory.

The system is governed by the following equation of motion:

$$q_t + J(\psi, q) = F + D, \tag{1.1}$$

where the quasigeostrophic potential vorticity, q, is related to the streamfunction ψ through

$$q = \Delta\psi - \lambda^2\psi, \tag{1.2}$$

and where $\lambda = L_D^{-1}$ is the inverse Rossby deformation length. The terms F and D represent forcing and damping, respectively: F may represent the input of energy into the system from large-scale instabilities, or from small-scale convective motions, while D may represent the dissipation of energy at large scales by flow over rough topography or from radiative transfer processes, as discussed below.

When $L_D/L \gg 1$, where L is a typical length scale of the flow, such as the scale at which the forcing is dominant, the evolution of (1.1) is practically indistinguishable from the two-dimensional Euler equations. Phenomenological and numerical studies of (1.1) have tended to focus on the opposite situation in which $L_D/L \ll 1$ (e.g. Larichev & McWilliams 1991; Iwayama, Shepherd & Watanabe 2002; Smith *et al.* 2002), which allows certain asymptotic results to be obtained, including scaling laws for the increase in dynamical time scales with increasing λ. No scaling laws have been derived or empirically deduced for the intermediate case $L_D/L \sim O(1)$, even for fundamental quantities such as the ratio of kinetic and potential energies at statistical equilibrium, or the halting scale of the inverse energy cascade by large-scale dissipation. These two quantities are the focus of the current paper.

Two essentially distinct forms of large-scale dissipation can be considered as relevant, according to the physical situation, which may be motivated by consideration of the rotating shallow-water system of equations from which (1.1) is derived. The shallow-water equations can be viewed as describing the motion of a shallow layer of rotating fluid, of mean layer depth H, or, alternatively, as describing an internal vertical mode of equivalent depth H in a continuously stratified fluid. In the shallow-water system, the effect of bottom friction may be represented simply by a linear drag on the velocity, $\boldsymbol{u}$, in the horizontal momentum equations. The effect of long-wave cooling, the dissipation mechanism most relevant to the motions of planetary atmospheres, may be represented by a Newtonian cooling in the thermodynamic equation (e.g. Andrews, Holton & Leovy 1987), which in the shallow-water system is equivalent to a relaxation on the height field h. Thus,

$$\boldsymbol{u}_t + \boldsymbol{u}\cdot\boldsymbol{\nabla}\boldsymbol{u} + f\boldsymbol{k}\times\boldsymbol{u} = -g\boldsymbol{\nabla}h - r\boldsymbol{u}, \tag{1.3a}$$

$$h_t + \boldsymbol{\nabla}\cdot(\boldsymbol{u}h) = -\alpha(h - H), \tag{1.3b}$$

where r is the frictional damping rate, α is the thermal damping rate, and $\boldsymbol{k}$ is the unit vector in the vertical direction. The system (1.3) can be combined to form an evolution equation for the potential vorticity, $Q = (\zeta + f)/h$,

$$Q_t + \boldsymbol{u}\cdot\boldsymbol{\nabla}Q = \alpha Q h'/h - r\zeta, \tag{1.4}$$

where $\zeta = \boldsymbol{k}\cdot\boldsymbol{\nabla}\times\boldsymbol{u}$ is the vorticity and $h' = h - H$ is the height perturbation. Note that Q is materially conserved when $\alpha = r = 0$. Under the usual quasigeostrophic

approximation, and defining the quasigeostrophic streamfunction $\psi = gh'/f$, (1.4) reduces to (1.1) and (1.2) with

$$D = \alpha\lambda^2\psi - r\Delta\psi. \tag{1.5}$$

This paper is mainly concerned with the case of thermal damping $\alpha \neq 0$, $r = 0$. As is discussed in § 2 below, the case of purely frictional damping does not in general lead to a stationary state, since equilibration of potential energy requires a dissipation mechanism more active at large scales. In § 3, we consider the equilibration of energy and the scale at which equilibration occurs when thermal damping is used, discussing simple phenomenological predictions and presenting numerical support for a refined scaling law. In § 4, we consider briefly the effect of the scale-selective nature of thermal damping on the inverse cascade: distortion of the energy spectrum is obtained in all cases but in a way that is largely independent of λ. Conclusions are given in § 5.

2. Energy equilibration

2.1. *Partition of kinetic and potential energy*

In the inviscid limit (1.1), equilibrium consists of a balance between energy input by F and large-scale dissipation by D. Multiplying (1.1) by $-\psi$ and integrating over the domain yields

$$\dot{\mathscr{E}} = -2r\mathscr{T} - 2\alpha\mathscr{P} + \varepsilon, \tag{2.1}$$

where ε is the rate of energy input and where $\mathscr{E} = -\int \psi q \,\mathrm{d}A$, $\mathscr{T} = -\int \psi\zeta \,\mathrm{d}A$, and $\mathscr{P} = \int \lambda^2\psi^2 \,\mathrm{d}A$ are the domain-integrated total, kinetic and potential energies, respectively. In the undamped case $r = \alpha = 0$, energy increases linearly at rate ε, but the distribution between $\mathscr{T}$ and $\mathscr{P}$ is not predicted. An approximate partition may be obtained from the identity

$$\lambda^2 T(k) = k^2 P(k) \tag{2.2}$$

where $T(k)$ and $P(k)$ are the kinetic and potential energy spectra, and k is the wavenumber. If it is assumed that the spectra are peaked at a distinct wavenumber k_p then (2.2) may be integrated to yield

$$\lambda^2\mathscr{T} \sim k_p^2\mathscr{P}. \tag{2.3}$$

The ratio of kinetic to potential energy thus depends on the ratio of the energy peak wavenumber k_p and inverse deformation length λ.

For illustration, figure 1(*a*) shows the growth in time of kinetic (solid line) and potential (dotted line) energy for representative integrations of (1.1) for values of $\lambda = 0.5, 1, 2, 4, 8, 16$. In these integrations F is an isotropic, band-limited stochastic forcing, delta-correlated in time, of Fourier modes $\boldsymbol{k}$ satisfying $|k - k_f| \leqslant \delta_f$ centred on wavenumber $k_f = 32$ with width $\delta_f = k_f/16$. The energy input rate $\varepsilon = 1$. The integration uses a standard pseudo-spectral algorithm with a fourth-order Runge–Kutta time-stepping scheme, and a periodic domain of size $2\pi \times 2\pi$ with $N = 1024$ grid points in each direction. De-aliasing is by way of a spectral filter, giving a maximum resolved wavenumber of $k_{max} = 3N/8 = 384$, and a weak fourth-order Laplacian hyperdiffusion controls the enstrophy at small scales. The choice of parameters gives a value of $k_{max}/k_f = 12$ large enough that forcing scales are adequately resolved (Scott 2007) and ensures that almost all of the energy input is transferred to larger scales

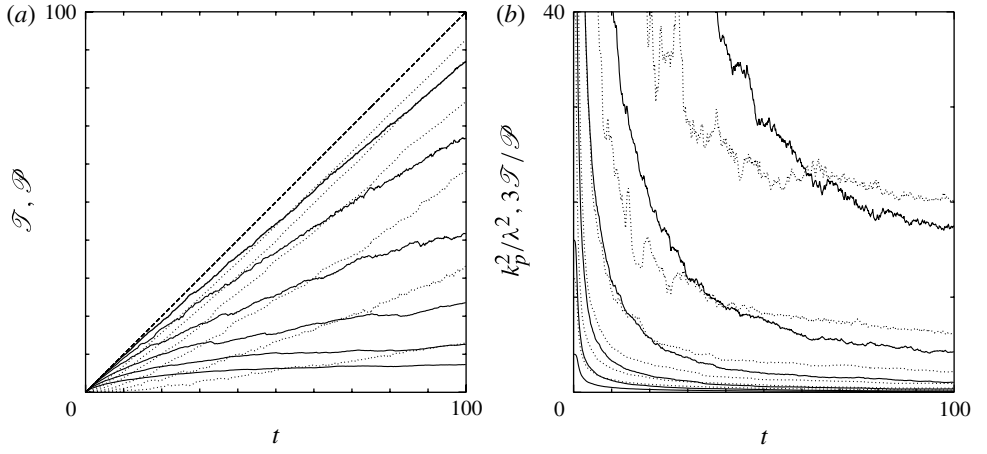

FIGURE 1. (*a*) Kinetic energy (solid) and potential energy (dotted) as a function of time, obtained from integrations of (1.1) with $D = 0$, and $\lambda = 0.5, 1, 2, 4, 8, 16$. (*b*) The ratio k_p^2/λ^2 (solid), where k_p is the energy centroid (2.4), and $\mathscr{T}/\mathscr{P}$ (dotted). In (*a*) lines of $\mathscr{T}$ are lower in the plot for larger λ, corresponding lines of $\mathscr{P}$ are higher; in (*b*) lines of k_p/λ and $\mathscr{T}/\mathscr{P}$ are both lower at larger values of λ.

with minimal loss to hyperdiffusion. Higher resolution integrations and the effects of varying k_f and k_{max} are considered in more detail in §§ 3 and 4.

In figure 1(*a*), $\mathscr{T}$ and $\mathscr{P}$ are scaled by the fraction of ε, ε_{eff}, that is transferred to large scales, to account for the small fraction of ε that is lost to hyperdiffusion (typically less than a few per cent). The growth of total energy at rate $\varepsilon = 1$ is represented by the straight dashed line with unit slope. At early time growth of kinetic energy follows growth of total energy, until significant energy builds up at scales close to L_D. At this time, which occurs earlier at higher values of λ, growth of kinetic energy slows, while growth of potential energy increases: at late time and large λ almost all energy growth is associated with increasing $\mathscr{P}$.

As shown in figure 1(*b*), the change in the ratio of kinetic and potential energy approximately follows the evolution of the peak wavenumber k_p, the latter represented here simply by the wavenumber centroid of the energy spectrum:

$$k_p = \frac{\int kE(k)\,\mathrm{d}k}{\int E(k)\,\mathrm{d}k}. \tag{2.4}$$

When $k_p \ll \lambda$ the time evolution of k_p/λ is close to the scaling $k_p/\lambda \sim \lambda^{-1/4}\varepsilon^{1/3}t^{-3/8}$ suggested by Watanabe, Fujisaka & Iwayama (1997), although the observed dependence on λ appears to be significantly stronger. We note that due to saturation of the energy at the domain scale, we do not expect exact agreement between $\mathscr{T}/\mathscr{P}$ and k_p/λ here. More detailed comparison will be made in § 3 below for cases in which large-scale dissipation allows equilibration at scales well below the domain scale.

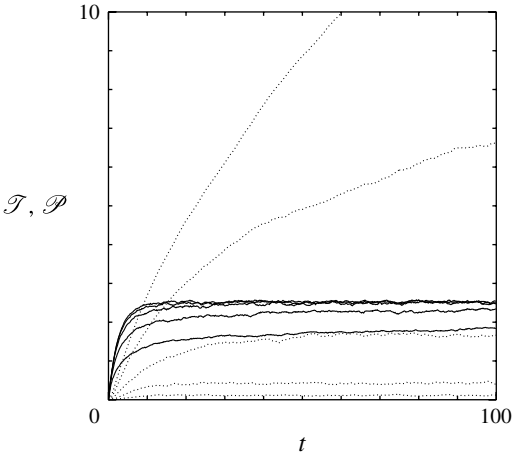

FIGURE 2. Kinetic energy (solid) and potential energy (dotted) as a function of time, obtained from integrations of (1.1) with $\lambda = 1, 2, 4, 8, 16$ and D given by (1.5) with $r = 0.2$, $\alpha = 0$. Lines of $\mathscr{T}$ are lower in the plot for larger λ, corresponding lines of $\mathscr{P}$ are higher.

2.2. *Frictional dissipation*

Frictional dissipation has been widely used in studies of two-dimensional barotropic turbulence ($\lambda = 0$), in part because it allows a convenient energy closure, although it has the drawback of damping vorticity equally across scales, thereby preventing a true inertial range (Sukorianski, Galperin & Chekhlov 1999). For the case $\lambda \neq 0$ considered here, (2.1) with $r \neq 0$, $\alpha = 0$ gives at equilibrium the balance

$$\mathscr{T} = \varepsilon/2r. \tag{2.5}$$

Unlike the barotropic case, however, there is no property of (2.1) that indicates a stationary state should be reached. Assuming that $\dot{\mathscr{T}}$ and $\dot{\mathscr{P}}$ are both positive definite, the most that can be inferred from (2.1) is that $\mathscr{T}$ will equilibrate at a value $\mathscr{T} \leqslant \varepsilon/2r$, while $\mathscr{P}$ may continue growing indefinitely at rate $\dot{\mathscr{P}} = \varepsilon - 2r\mathscr{T}$, at least until the domain scale is reached. Such growth in $\mathscr{P}$ would be associated with a redistribution of kinetic energy to larger scales in accordance with the relation (2.2).

Figure 2 shows the kinetic and potential energy for integrations of (1.1) and (1.5) with $r = 0.2$, $\alpha = 0$. For $\lambda = 1, 2, 4$ equilibration occurs on a time scale of approximately $1/r = 5$, with $\mathscr{T}$ close to the predicted value of $\varepsilon/2r = 2.5$. For larger λ, equilibration has not yet occurred by $t = 100$: values of $\mathscr{T}$ remain measurably below the predicted value and accordingly the potential energy shows continued growth over this period. It is likely that over sufficiently long time scales equilibrium will be reached as the potential energy peak reaches the domain scale and further redistribution of $T(k)$ is restricted. It is not clear, and difficult to test computationally, whether complete equilibration of $T(k)$ and $\mathscr{P}$ would ever occur in an unbounded domain.

2.3. *Thermal damping*

Thermal relaxation is the most physically relevant form of energy dissipation for studies of the middle atmosphere, or of the atmospheres of the gas giant planets,

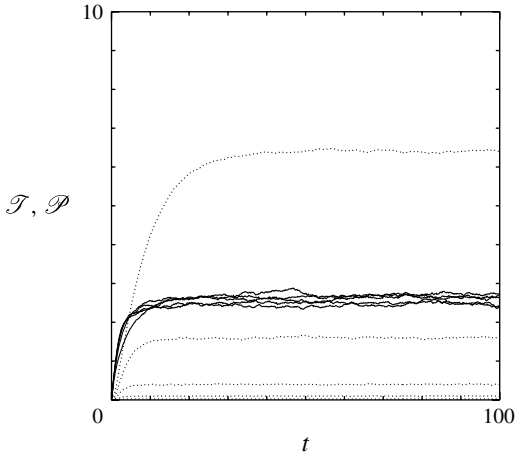

FIGURE 3. As figure 2 but with thermal damping at rate $\alpha = 20/\lambda^2$.

where there is no frictional boundary layer overlying a lower solid surface; it is known to be the main mechanism for energy dissipation in the terrestrial stratosphere (e.g. Andrews *et al.* 1987). Recent studies of global shallow-water turbulence on a sphere have indicated that the form of large-scale dissipation can determine the nature of equatorial jets, with thermal damping favouring equatorial super-rotation (Scott & Polvani 2007, 2008) consistent with the sense of the equatorial jets on the gas giant planets. In the analysis of the inverse energy cascade, thermal damping may also be a favourable choice: in contrast to frictional dissipation, it is scale-selective, acting predominantly at large scales, and may thus, in principle, avoid the frictional contamination of the inertial range observed by Sukorianski *et al.* (1999), although, as shown in § 4 below, it is nevertheless subject to bottleneck effects and spectral steepening similar to that found with high-order hypodiffusive operators considered by Borue (1994) and Danilov & Gurarie (2001).

At equilibrium, (2.1) with $r = 0$, $\alpha \neq 0$ gives the balance

$$\mathscr{P} = \varepsilon/2\alpha. \tag{2.6}$$

At first sight this does not appear to offer any advantages over the frictional damping case considered above, since now (1.1) does not constrain $\mathscr{T}$. Use may be made, however, of the identity (2.2) together with the fact that energy cascades to larger-scales. Since, through (2.2), $\mathscr{P}$ may be considered to be a larger-scale quantity than $\mathscr{T}$, equilibration of $\mathscr{P}$ will necessarily constrain values of $\mathscr{T}$: in particular, no $\mathscr{P}$-preserving rearrangement of $P(k)$ is possible in which there is both a transfer of total energy to larger-scales and a simultaneous increase of $\mathscr{T}$.

Figure 3 shows the kinetic and potential energy for cases similar to those in figure 2 but with thermal damping at rate $\alpha = 20/\lambda^2$ (and $r = 0$). This value was chosen empirically to give approximately the same values for the equilibrated kinetic energy as the previous case $r = 0.2, \alpha = 0$. The time scale for equilibration of $\mathscr{T}$ is here also similar to the previous case. Note from (1.5) that scaling α with λ^{-2} ensures comparable damping of the streamfunction across different values of λ, and results in the comparable values of equilibrated $\mathscr{T}$, which are almost indistinguishable in

figure 3. Note, again, that values of both $\mathscr{T}$ and $\mathscr{P}$ are scaled by ε_{eff} to account for the small amount of energy input lost to hyperdiffusion at small scales. The important point here, however, is that, in contrast to the case of frictional damping, the potential energy $\mathscr{P}$ reaches a steady value in all cases. Equilibrium values of $\mathscr{P}$ scale as λ^2 in accordance with (2.6). The approximate relation (2.3) thus describes the energy equilibration reasonably accurately across this range of λ.

3. Halting scale and energy partition

The scaling of $\mathscr{T}/\mathscr{P}$ with λ^{-2} holds in the above integrations because the peak in the energy spectrum occurs at similar wavenumbers k_p across all values of λ. A more complete description of the partition between $\mathscr{T}$ and $\mathscr{P}$ requires an estimate of k_p for different values of the large-scale dissipation rates α or r. Due to the lack of equilibration when $\alpha = 0$, we restrict attention here to the case $r = 0$, $\alpha > 0$, which gives clear equilibration of both $\mathscr{T}$ and $\mathscr{P}$.

It is useful to consider the four main parameters that govern the system (1.1) with the form of forcing and dissipation used here: λ, ε, α and k_f. These may be combined into two non-dimensional parameters that control the behaviour of the system:

$$\gamma_1 = \varepsilon\lambda^2/\alpha^3 \quad \text{and} \quad \gamma_2 = \lambda/k_f. \tag{3.1}$$

These two parameters completely specify the system up to a rescaling of time or space: different values of the physical parameters that leave γ_1, γ_2 unchanged correspond simply to different time and length scales, but are otherwise equivalent. The parameters in the numerical integrations presented below have been chosen such that the maximum and minimum length scales imposed by the domain and resolution are respectively much larger and smaller than typical length scales of the flow.

If it assumed that the forcing scale is sufficiently small that $\gamma_2 \ll 1$, and that γ_2 consequently has no effect on the evolution, then k_p/λ can depend only on γ_1. An estimate for k_p in terms of γ_1 was suggested previously by Smith *et al.* (2002) for the case $k_p \ll \lambda$, termed large-scale quasigeostrophic flow, based on a comparison of typical damping and advective time scales. We begin by noting that in fact the same estimate holds also in the other limit, namely when $k_p \gg \lambda$. In this case, the right-hand side of (1.5) gives the damping time scale of motions at scale k_p^{-1} as

$$\tau_{rad} \sim (k_p^2 + \lambda^2)/\alpha\lambda^2 \sim k_p^2/\alpha\lambda^2, \tag{3.2}$$

while for the advective time scale

$$\tau_{adv} \sim [k_p^3 T(k_p)]^{-1/2} \tag{3.3}$$

may be taken with an assumed Kolmogorov–Kraichnan (Kraichnan 1967) kinetic energy spectrum of the form $T(k) \sim \varepsilon^{2/3}k^{-5/3}$. Combining (3.2) and (3.3) yields $k_p \sim (\alpha^3\lambda^6/\varepsilon)^{1/8}$, or

$$k_p/\lambda \sim \gamma_1^{-1/8}, \tag{3.4}$$

which is the same as the estimate obtained by Smith *et al.* (2002) (equation (5.7*c*), therein), but valid in the range $k_p \gg \lambda$ rather than $k_p \ll \lambda$. The same estimate may also be obtained without reference to the slope of the energy spectrum using the simpler

$$\tau_{adv} \sim (k_p U)^{-1}, \tag{3.5}$$

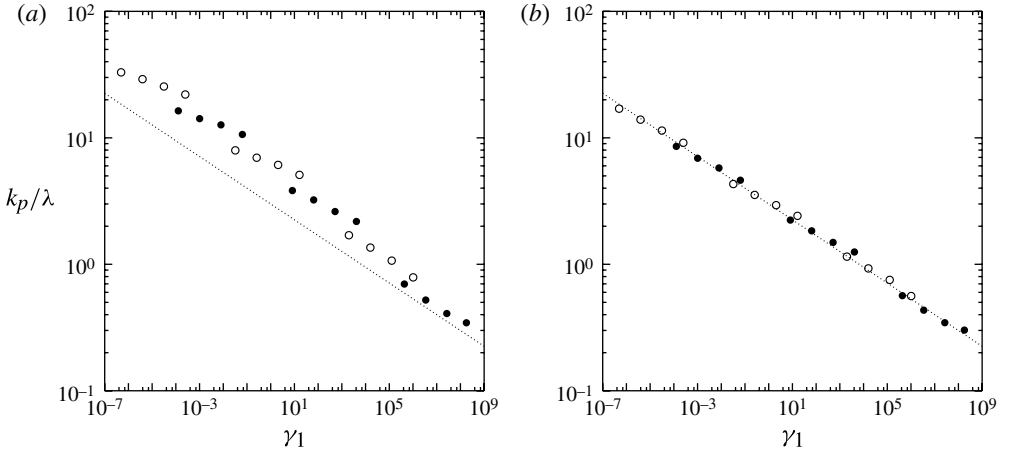

FIGURE 4. Ratio k_p/λ against γ_1. In (a) k_p is the full energy centroid (2.4); in (b) it is the centroid of the potential energy spectrum, defined analogously. Dotted lines indicate the slope $-1/8$. Each group of four filled or open circles indicates a separate value of λ, higher values of λ to the right; values of α decrease to the right within each group.

where U is a characteristic velocity, which may be taken here as $\mathscr{T}^{1/2}$, and using the relations (2.3) and (2.6). Since thermal damping is effectively a dissipation on the streamfunction, the quantity k_p in (3.2) and (3.5) should be taken to be the centroid of the potential energy spectrum $P(k)$, rather than that of the full spectrum $E(k)$.

The estimate (3.4) has not been very well supported by numerical computations. For the situation of $k_p \ll \lambda$, Smith *et al.* (2002) computed the peak in the energy spectrum (rather than the centroid) and found reasonable agreement with the estimate (3.4), but with a dependence of k_p on α somewhat stronger than suggested by (3.4). The dependence on λ was not considered. Figure 4 shows the results from a series of integrations across all combinations of the values $\lambda = 0.5, 1, 2, 4, 8, 16$ and $\alpha\lambda^2 = 2.5, 5, 10, 20$, for which we cover the regime $k_p \ll \lambda$ as well as extending across into $k_p \gg \lambda$. For each calculation equilibration of $\mathscr{P}$ and $\mathscr{T}$ was verified (equilibration was marginal for the case $\lambda = 16$ and $\alpha = 2.5$ but otherwise achieved well before the end of the integrations at $T = 100$). The value of k_p was computed from both the full energy centroid (2.4) (figure 4*a*) and the potential energy centroid (figure 4*b*), averaged over the last 20 % of each integration, and the value of k_p/λ plotted against γ_1. As in Smith *et al.* (2002), the agreement is reasonable but not perfect. In particular, within each group of simulations with a given λ (groups of filled or open circles), there is a systematic departure from the predicted scaling with α, suggesting a somewhat shallower power-law dependence. The scaling of the data with λ follows (3.4) more closely across the full range of k_p/λ, particularly when k_p is taken to be the centroid of the potential energy spectrum.

An improved scaling may be obtained by retaining a possible dependence on k_f through the parameter γ_2. We make the observation that (3.4) holds well for values of α and λ such that $\alpha\lambda^2$ is fixed; this corresponds simply to k_p being independent of λ for fixed $\alpha\lambda^2$, the coefficient of dissipation in (1.5). Equation (3.4) may then be

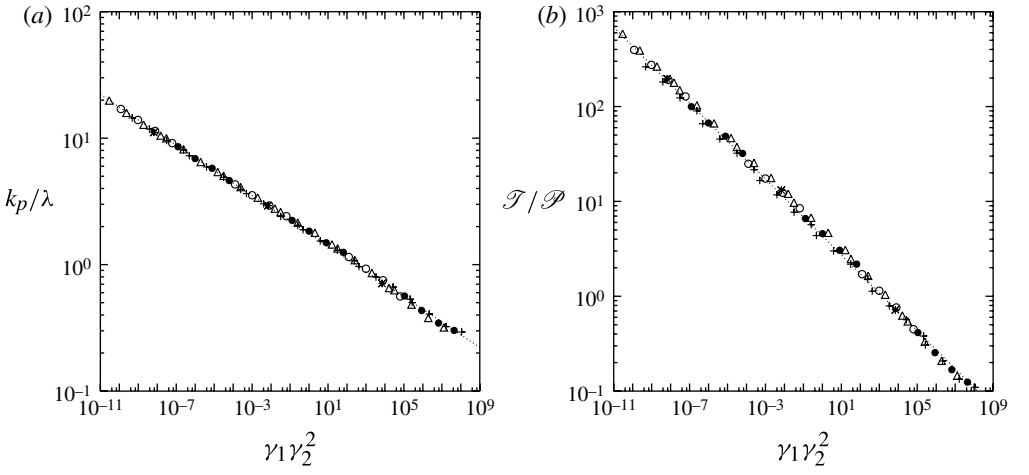

FIGURE 5. Ratios (*a*) k_p/λ and (*b*) $\mathscr{T}/\mathscr{P}$ against $\gamma_1\gamma_2^2$, with k_p obtained from the centroid of the potential energy spectrum. Dotted lines indicate the slopes $-1/10$ and $-1/5$ in (*a*) and (*b*), respectively. Filled and open circles denote $k_f = 32$ as in figure 4; crosses denote $k_f = 16$, triangles denote $k_f = 64$, stars denote $k_f = 128$.

generalized to

$$k_p/\lambda = C(\beta)\gamma_1^{-1/8}, \tag{3.6}$$

where $C(\beta)$ is a non-universal prefactor and $\beta = \varepsilon k_f^8/\alpha^3\lambda^6 = \gamma_1/\gamma_2^8$ is the unique non-dimensional combination of the parameters ε, k_f and $\alpha\lambda^2$. In particular, the choice $C(\beta) = \beta^{1/40}$ yields

$$k_p/\lambda \sim (\gamma_1\gamma_2^2)^{-1/10}, \tag{3.7}$$

which has a shallower dependence on α than (3.4) and provides a remarkably good fit to the numerical data, as shown in figure 5(*a*). This scaling has been verified by performing additional integrations of all the above cases with the values $k_f = 16, 32, 64$ (at grid resolutions 512, 1024, 2048 to keep the ratio $k_{max}/k_f = 12$ fixed), as well as a selection of cases with $k_f = 128$. Figure 5(*a*) shows all values of k_p/λ plotted against $\gamma_1\gamma_2^2$, and indicates good agreement with a $-1/10$ power law, again over the full range of parameters, and for all values of k_f. We note that the scaling obtained here holds across a wide range of k_p/λ, from $k_p \gg \lambda$ to the $k_p \ll \lambda$ limit considered by Smith *et al.* (2002). A least-squares linear regression of the data indicates $k_p/\lambda = C_h(\gamma_1\gamma_2^2)^p$, with $p = -0.099$ and prefactor $C_h = 1.76$, with a chi-square goodness-of-fit of 0.045. Fitting to the more general $k_p/\lambda = C_h(\gamma_1^p\gamma_2^q)$ suggested a possibly lower value for q of -0.176, but with an almost negligible improvement of the goodness-of-fit to 0.040.

Finally, the partition between kinetic and potential energy may be obtained from (2.3) and (3.7), giving

$$\mathscr{T}/\mathscr{P} \sim (\gamma_1\gamma_2^2)^{-1/5}. \tag{3.8}$$

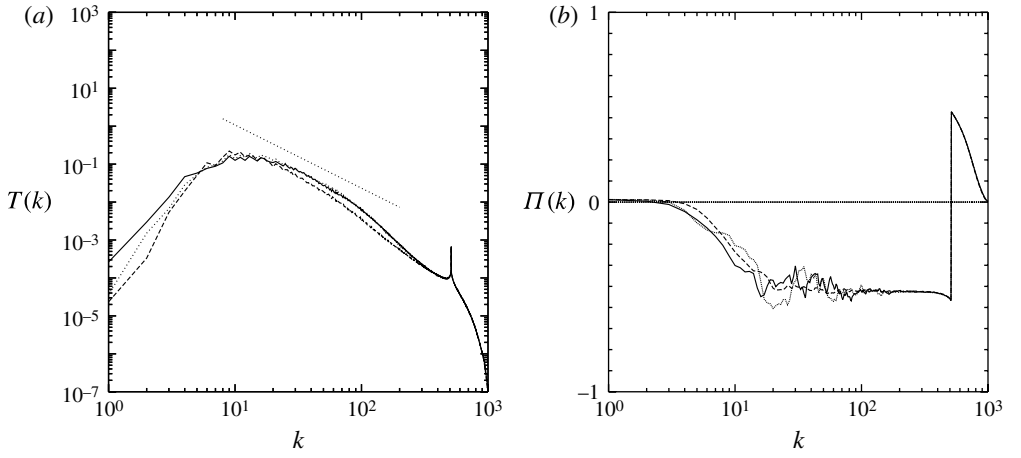

FIGURE 6. (*a*) Kinetic energy spectrum $T(k)$ and (*b*) energy flux $\Pi(k)$ for integrations with $k_f = 512$, $\alpha\lambda^2 = 10$, and $\lambda = 1, 4, 16$ (solid, dotted, and dashed, respectively). The straight dotted line in (*a*) indicates the slope $-5/3$ for reference only.

Values of $\mathscr{T}/\mathscr{P}$ for the simulations described above are plotted in figure 5(*b*), and indicate good agreement with (3.8) across all parameter values. A least-squares fit to $\mathscr{T}/\mathscr{P} = C_e\,(\gamma_1\gamma_2^2)^p$ here gives $p \approx -0.20$ and $C_e \approx 4.30$, with a chi-square goodness-of-fit of 0.196. Again, the form of (3.7) is such that k_p depends on α and λ only in the combination $\alpha\lambda^2$. Since $\mathscr{P} = \varepsilon/2\alpha$, it follows from (2.3) that $\mathscr{T}$ also depends only on the combination $\alpha\lambda^2$, consistent with the uniform energy levels obtained in the integrations shown in figure 3, for which $\alpha \propto \lambda^{-2}$.

4. Inertial-range properties

In view of the similarity to atmospheric radiative damping, we consider briefly the structure of the inverse energy cascade at equilibrium. Borue (1994) noted the large-scale condensation and steepening of the energy spectrum that occurs in two-dimensional barotropic turbulence when energy dissipation is confined to the lowest wavenumbers. Danilov & Gurarie (2001) further showed the incompatibility of a constant-flux energy inertial range with the Kolmogorov–Kraichnan $k^{-5/3}$ energy spectrum. In effect, the thermal damping of (1.5) with $\alpha > 0$ may be considered as a hypodiffusive operator in the limit $\lambda \to 0$ such that the coefficient $\alpha\lambda^2$ retains a finite value, and so distortion of the inverse cascade is also expected in this case.

Figure 6(*a*) shows the kinetic energy spectrum, $T(k)$, for three cases $\lambda = 1, 4, 16$ and with forcing at wavenumber $k_f = 512$. In all cases there is significant distortion of the Kolmogorov–Kraichnan spectrum, with elevated energy levels across a range of intermediate wavenumbers extending from k_p towards k_f and steeper spectral slopes near k_f; the form is similar to spectra obtained in other studies (e.g. Borue 1994; Danilov & Gurarie 2001). Perhaps surprisingly, there is little dependence on λ across the range considered, apart from a slight flattening at $\lambda = 16$: this suggests that the large-scale condensation arising from the scale-selective dissipation may be a more important effect than any condensation associated with the finite deformation radius, at least over the parameter range considered here. Figure 6(*b*) shows the energy flux,

exhibiting the constant flux range where thermal dissipation has no effect on the energy cascade. The reduction from $\Pi(k) = \varepsilon$ is due to significant energy dissipation in the vicinity of the forcing scales for the high value of k_f used in these cases.

5. Conclusions

In the quasigeostrophic system (1.1) with finite deformation radius and constant energy input at small scales, energy dissipation must be scale-selective to guarantee equilibration of total energy at scales below the domain scale. In particular, linear friction, which controls the kinetic energy equilibrium places no constraint on potential energy, which may grow unrestricted until saturation at the domain scale. Thermal damping is a natural dissipation mechanism, closely related to long-wave cooling in the atmosphere, that ensures equilibration of both potential energy and kinetic energy.

Equilibrium levels of kinetic and potential energy are related through the approximate partition (2.3), where k_p is a suitably defined halting scale of the inverse cascade that may depend on a combination of two non-dimensional parameters γ_1 and γ_2 given by (3.1). Simple dimensional arguments give $k_p/\lambda \sim \gamma_1^{-1/8}$, over a range of k_p/λ not restricted to the $k_p \ll \lambda$ limit considered by Smith *et al.* (2002); this scaling captures the dependence on λ (not considered by Smith *et al.*) but overestimates the dependence on α. On the other hand, based on a large number of integrations of (1.1) the halting scale is found to be better estimated by $k_p/\lambda = C_h\,(\gamma_1\gamma_2^2)^{-1/10}$, with prefactor $C_h \approx 1.76$ obtained from a least-squares fit. At present there is no adequate theory for the value of the prefactor, nor for the suggested dependence on k_f that arises through $\gamma_2 = \lambda/k_f$. The estimate for the halting scale gives immediately an estimate for the partition between kinetic and potential energy $\mathscr{T}/\mathscr{P} = C_e\,(\gamma_1\gamma_2^2)^{-1/5}$, with prefactor $C_e \approx 4.30$ again obtained from a least-squares fit.

The scale-selective nature of thermal damping produces a large-scale bottleneck in the inverse cascade and a steepening of the energy spectrum, similar to that found in the two-dimensional barotropic system with high-order hypodiffusive dissipation. The distortion of the energy spectrum is largely independent of λ for values in a range around k_p, suggesting that the bottleneck effect arising from the damping is more important than that arising from a reduction of the energy cascade by λ.

Acknowledgements

Support for this research was provided by the National Science Foundation (R.K.S.) and by a Leverhulme Trust Research Fellowship (D.G.D.).

References

ANDREWS, D. G., HOLTON, J. R. & LEOVY, C. B. 1987 *Middle Atmosphere Dynamics*. Academic.

BORUE, V. 1994 Inverse energy cascade in stationary two-dimensional homogeneous turbulence. *Phys. Rev. Lett.* **72**, 1475–1478.

DANILOV, S. & GURARIE, D. 2001 Nonuniversal features of forced two-dimensional turbulence in the energy range. *Phys. Rev.* E **63**, 020203(R).

HASEGAWA, A. & MIMA, K. 1978 Pseudo-three-dimensional turbulence in magnetized nonuniform plasma. *Phys. Fluids* **21**, 87–92.

IWAYAMA, T., SHEPHERD, T. G. & WATANABE, T. 2002 An 'ideal' form of decaying two-dimensional turbulence. *J. Fluid. Mech.* **456**, 183–198.

KRAICHNAN, R. H. 1967 Inertial ranges in two-dimensional turbulence. *Phys. Fluids* **10**, 1417–1423.

LARICHEV, V. D. & MCWILLIAMS, J. C. 1991 Weakly-decaying turbulence in an equivalent barotropic fluid. *Phys. Fluids* A **3**, 938–950.

SCOTT, R. K. 2007 Non-robustness of the two-dimensional turbulent inverse cascade. *Phys. Rev.* E **75**, 046301.

SCOTT, R. K. & POLVANI, L. M. 2007 Forced-dissipative shallow-water turbulence on the sphere and the atmospheric circulation of the gas planets. *J. Atmos. Sci.* **64**, 3158–3176.

SCOTT, R. K. & POLVANI, L. M. 2008 Equatorial superrotation in shallow atmospheres. *Geophys. Res. Lett.* **35**, L24202.

SMITH, K. S., BOCCALETTI, G., HENNING, C. C., MARINOV, I., TAM, C. Y., HELD, I. M. & VALLIS, G. K. 2002 Turbulent diffusion in the geostrophic inverse cascade. *J. Fluid Mech.* **469**, 13–48.

SUKORIANSKI, S., GALPERIN, B. & CHEKHLOV, A. 1999 Large scale drag represention in simulations of two-dimensional turbulence. *Phys. Fluids* **11**, 3043–3053.

VALLIS, G. K. 2006 *Atmospheric and Oceanic Fluid Dynamics*. Cambridge University Press.

WATANABE, T., FUJISAKA, H. & IWAYAMA, T. 1997 Dynamical scaling law in the development of drift wave turbulence. *Phys. Rev.* E **55**, 5575–5580.